GEOCHEMISTRY

Complex carbonaceous matter in Tissint martian meteorites give insights into the diversity of organic geochemistry on Mars

Philippe Schmitt-Kopplin[1,2,3]*, Marco Matzka[3], Alexander Ruf[1,4,5], Benedicte Menez[6], Hasnaa Chennaoui Aoudjehane[7], Mourad Harir[3], Marianna Lucio[3], Jasmine Hertzog[1,3], Norbert Hertkorn[3], Régis D. Gougeon[8], Victor Hoffmann[9], Nancy W. Hinman[10], Ludovic Ferrière[11], Ansgar Greshake[12], Zelimir Gabelica[13], László Trif[14], Andrew Steele[15]

We report a huge organic diversity in the Tissint Mars meteorite and the sampling of several mineralogical lithologies, which revealed that the organic molecules were nonuniformly distributed in functionality and abundance. The range of organics in Tissint meteorite were abundant $C_{3\text{-}7}$ aliphatic branched carboxylic acids and aldehydes, olefins, and polyaromatics with and without heteroatoms in a homologous oxidation structural continuum. Organomagnesium compounds were extremely abundant in olivine macrocrystals and in the melt veins, reflecting specific organo-synsthesis processes in close interaction with the magnesium silicates and temperature stresses, as previously observed. The diverse chemistry and abundance in complex molecules reveal heterogeneity in organic speciation within the minerals grown in the martian mantle and crust that may have evolved over geological time.

INTRODUCTION

Mars and Earth share critical aspects of their gross planetary evolution, and while life evolved on Earth, the issue of probable past and current martian life is the subject of intense research by landed and orbital assets at Mars. Water and organic molecules, the key prerequisites for habitability and evolution of life, have been detected on Mars, and habitable zones in the deep martian subsurface potentially suitable for microbial life have been proposed (*1*–*4*). The presence of transient methane, refractory organic molecules, and halogenated/sulfur-functionalized aliphatic/aromatic compounds on Mars has also been found (*1*, *4*–*6*). Discussion as to the origin of these molecules is still ongoing.

Combustion analysis of the cryoconserved Antarctic martian meteorite (EETA 79001) already indicated the presence of noncarbonate Mars endogenous carbonaceous compounds 30 years ago (*7*). The Antarctic meteorite ALH 84001 attracted special interest and controversy in the late 1990s because morphologies detected by electron microscopy were attributed to microfossils (*8*), an interpretation criticized later (*9*). Analytical techniques, such as pyrolysis–gas chromatography–mass spectrometry (Py-GC-MS), confirmed the presence of high–molecular weight organic matter in Nakhla and ALH 84001 martian meteorites but which could not be distinguished from contamination (*10*), and graphite was described with transmission electron microscopy and Raman in ALH 84001 (*11*). Most recently, complex refractory organic material associated with mineral assemblages was shown to be formed by mineral carbonation and serpentinization reactions within water-rock interactions (*12*). Additional abiotic reduced carbon phases, including endogenous polycyclic aromatic hydrocarbons (PAHs) in other martian meteorites, were associated with high-temperature mineral inclusions, as observed by Raman spectroscopy and laser desorption MS (*13*). The provenance, formation, and implications of carbonaceous phases in martian meteorites were reviewed (*14*), and a recent hypothesis was proposed for organic synthesis through electrochemical reduction of CO_2 (*15*). Recent ^{13}C and ^{18}O measurements obtained on Mars by the Sample Analysis at Mars (SAM) instrument on Curiosity rover have revealed the presence of carbon in multiple phases (*2*), supplementing earlier in situ mass spectrometric detection of complex organic matter preserved in the 3-billion-year-old mudstone at Gale crater (*1*, *16*). The carbon derivatives previously identified on Mars itself and in martian meteorites were primarily known end-member–type repetitive materials, such as carbon allotropes, carbonates, and organic minerals. Raman spectroscopy, nanoscale secondary ion MS (NanoSIMS), and energy-dispersive x-ray (EDX) analysis, in conjunction with high-resolution imaging methods, provided assessment of macromolecular carbon phases and colocation with mineral phases (*15*, *17*) but could not discriminate components with molecular resolution, leaving open the challenge of understanding the evolution of molecular complexity and planetary habitability on Mars.

[1]Technische Universität München, Chair of Analytical Food Chemistry, Freising-Weihenstephan 85354, Germany. [2]Max Planck Institute for Extraterrestrial Physics, Center for Astrochemical Studies, Garching 85748, Germany. [3]Helmholtz München, Analytical BioGeoChemistry, Neuherberg 85764, Germany. [4]Excellence Cluster ORIGINS, Boltzmannstraße 2, Garching 85748, Germany. [5]Ludwig-Maximilians-University, Department of Chemistry and Pharmacy, Butenandtstr. 5-13, Munich 81377, Germany. [6]Université de Paris, Institut de Physique du Globe de Paris, CNRS - 1, rue Jussieu, Paris Cedex 05 75238, France. [7]Faculty of Sciences Ain Chock, GAIA Laboratory, Hassan II University of Casablanca, km 8 Route d'El Jadida, Casablanca 20150, Morocco. [8]UMR Procédés Alimentaires et Microbiologiques, Université de Bourgogne/AgroSupDijon, Institut Universitaire de la Vigne et du Vin Jules Guyot, Dijon 21000, France. [9]Faculty of Geosciences, Dep. Geo- and Environmental Sciences, LMU, Muenchen, Germany. [10]University of Montana, Missoula, MT 59812, USA. [11]Natural History Museum Vienna 1010, Austria. [12]Museum für Naturkunde Berlin, Berlin 10115, Germany. [13]Université de Haute Alsace, École Nationale Supérieure de Chimie de Mulhouse, F-68094 Mulhouse Cedex, France. [14]Research Centre for Natural Sciences, Institute of Materials and Environmental Chemistry, Budapest, Hungary. [15]Earth and Planetary Laboratory, Carnegie Institution for Science, 5251 Broad Branch Rd., Washington, DC 20015, USA.
*Corresponding author. Email: schmitt-kopplin@helmholtz-muenchen.de

Martian meteorites are primary igneous rocks subdivided into Shergottites (basaltic rocks), Nakhlites (cumulate clinopyroxenites), and Chassignites (dunites); ALH 84001 is an ancient cumulate orthopyroxenite, whereas most recently, NWA 7034 and its many pairings are regolith breccias (*14*, *18*). Their ejection ages are clustered, and trace element abundances as well as Sr-Nd isotope systematics suggest long-term evolution of mantle and crustal sources across martian geologic history, including differentiation of a martian magma ocean (*19*) and volcanism (*20*, *21*). To date, only five observed martian meteorite falls were recorded since 1815, with an average fall every 50 years, covering a wide range in petrological types and ejection ages from the planetary body. The Tissint meteorite is the most recent martian meteorite observed fall (18 July 2011 near the city of Tissint in Morocco) and comprises an olivine-phyritic shergottite of highly composite nature, with similarities to Antarctic meteorite EETA 79001 and with a crystallization age of 665 ± 74 million years (Ma), a preatmospheric radius of 22 ± 2 cm, and a cosmic ray exposure age of 0.9 ± 0.2 Ma (*22*). Tissint was described as bearing highly magnesian olivine macrocrysts in a fine matrix (*23*). More than 17 kg were recovered from this fall, with minor compositional variance between the recovered dozens of fragments; recovery starting days after the impact provided access to very fresh, contaminant-free material for organic analysis (*24*). Tissint meteorite comprises all high-pressure phases [seven minerals and two mineral glasses (*25*)] in unusually large sizes, indicating that shock metamorphism reached up to ~25 GPa and 2000°C and was widely dispersed in this sample. NanoSIMS, time-of-flight–SIMS, electron microscopy, and EDX previously demonstrated heterogeneous distribution of carbonaceous components in Tissint (*14*, *26*), which fill open fractures and are enclosed in shock melt veins, corroborating the complex history of their formation. A colocalization of carbon phases with magnesium silicates could also be observed in the samples analyzed here using electron microscopy and EDX (fig. S1), and these results corroborate recent studies with Allan Hills 84001, showing the colocation of reactive mineral and organic phases (*12*). Simultaneous thermal and mass spectrometric evolved gas [thermogravimetry–differential scanning calorimetry–mass spectrometric evolved gas analysis (TG-DSC-MSEGA)] measurements of Tissint revealed the very low mass loss from the sample up to 1000°C (Δm 1.52%). In the temperature interval up to 600°C, CO_2 [mass/charge ratio (m/z) 44] could be formed from the intramolecular redox reaction of organics, and other masses could result from the pyrolytic decomposition of some organics [m/z − 15 (CH_3+), 39 (C_3H_3+), and 41 (C_3H_5+)]. Above 600°C up to the end of the measurement, the formation of carbon dioxide and sulfur dioxide can also be detected, where the former could result from the decomposition of some carbonates, while the latter from the degradation of sulfates present in the sample (fig. S2). These results are in line with the latest results observed by the Mars Science Laboratory tunable laser spectrometer of the SAM, showing the production of CO_2, CH_4, CO, carbonyl sulfide, and CS_2 when pyrolyzing the samples from Gale crater on Mars and the Tissint sample (*27*) and with earlier results from the SAM instrument evolved gas analyzer that detected directly evolved water, H_2, SO_2, H_2S, NO, CO_2, CO, O_2, and HCl (*28*).

RESULTS

Least contaminated Tissint martian meteorite exhibits exceptional organic molecular diversity

We have investigated methanolic extracts from crushed specimens of the Tissint meteorite with electrospray ionization (ESI) and atmospheric photoionization (APPI) Fourier transform ion cyclotron resonance MS (FTICR-MS) and with proton-detected nuclear magnetic resonance (^{1}H NMR) spectroscopy, under analogous conditions to those described for meteorite soluble organic matter (SOM) (*29*, *30*). The extracts of fragments crushed in methanol, a polar protic solvent, comprise the most diverse complement of organic molecules available from soft extraction, which is intended to preserve the original speciation of organic molecules (*30*).

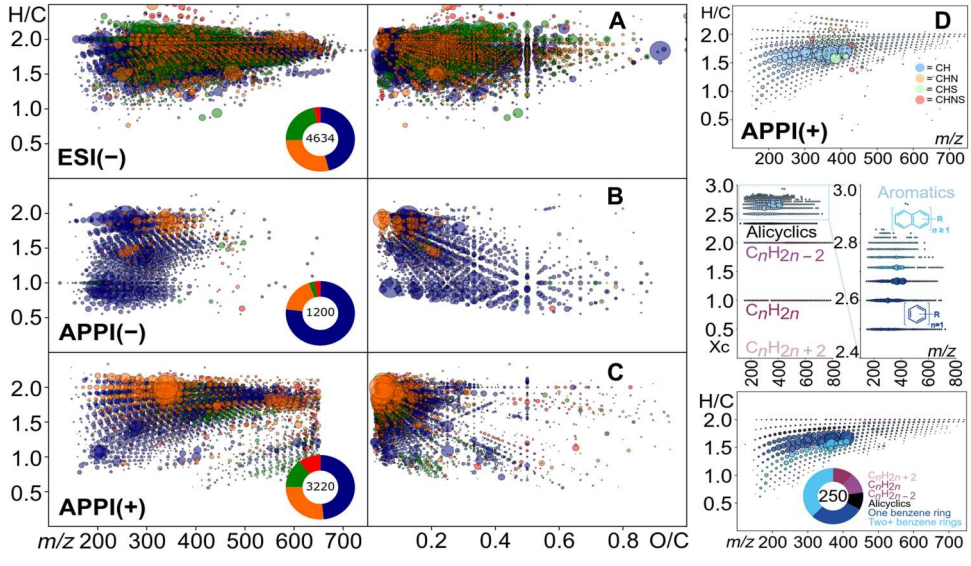

Fig. 1. FTICR-MS exact mass data converted in elementary composition and visualized in van Krevelen–type diagrams. (**A**) Electrospray (ESI) and (**B** to **D**) APPI FTMS–derived van Krevelen diagrams and mass-edited H/C ratios of CHNOS compounds in Tissint meteorite. Dot color in (A) to (C) refers to CHO (blue), CHNO (orange), CHOS (green), and CHNOS (red).

FTICR-MS analysis enables highly resolved ($R > 10^6$ at m/z 200) and accurate chemical mass analysis [<0.2 parts per million (ppm) mass accuracy] of ESI- and APPI-generated ions over a wide mass range from m/z 100 to 1000 (fig. S3). The Tissint methanolic extract showed a molecular atlas of more than 20,000 resolved mass signals in total, of which the monoisotopic masses were assigned to defined molecular compositions with the elements C, H, N, O, S, and Mg. The data visualization in van Krevelen diagram showed a typical meteoritic profile with abundance and chemical pattern reflecting a functional continuum of chemical homologous series in hydration, alkylations, hydroxylation, and carboxylations, as shown previously with various meteorites (Fig. 1). These observations of complex organic matter correlate with in situ observations of martian organic phases in Tissint by scanning transmission x-ray microscopy analyses, as shown in (*15*) and confirmed as martian in origin by hydrogen isotope analyses. We recently reported, with more than 60 chondrites and achondrites, that the SOM of meteorites is highly sensitive to metamorphism (pressure and temperature) (*31*): Not only does the abundance of organic species decrease along with the loss of volatile elements (C, H, N, O, and S) compared to pristine carbonaceous chondrites, but also, the number of nitrogen in N-bearing molecules increases, indicating internal chemical rearrangements (*32*, *33*). In addition, the abundance and structural diversity of high-pressure chemical markers dihydroxymagnesium carboxylates [$RCO_2Mg(OH)_2$] (CHOMg) progressively increased with shock metamorphism (*31*). Similarly, sulfur-bearing organomagnesium compounds [$RCO_2Mg(OH)_2SO_2$] (CHOSMg) were described as thermal-stress chemical witnesses in meteorites, enabling tracking of peak temperatures or long-duration thermal effects (*34*). The close relationships between respective CHO and CHO(S)Mg chemical spaces are thus dependent on pressure and temperature conditions and indicative of a coevolution of organic molecules and colocalized minerals in Mars rocks as well.

The negative electrospray FTICR mass spectra of the Tissint methanol extracts demonstrated the presence of more than 5000 assigned elementary compositions (considering the volatile elements C, H, N, O, S, and Mg), with relative counts in the order of CHO (38%) > CHNO (30%) > CHOS (20%) > CHNOS (11%) polar compounds. Organomagnesium [CHO(S)Mg] accounted for more than a hundred separate compounds. All of those arranged in extended, contiguous abundant molecular series across sizable ranges of mass (m/z ~150 to 700) and elemental ratios (fig. S4), indicating a well-evolved endogenous organic matter of considerable chemical diversity and chemosynthetic origin. CHO, CHOS, and CHNO compounds occupied similar ranges of polarity and saturation in the van Krevelen diagram (Fig. 1A), but CHO compounds showed the highest signal intensity and abundance. In comparison to carbonaceous chondrites methanol extracts (e.g., Murchison CM2), Tissint showed higher relative saturation, smaller signal intensity, and less oxygenation on average. We also analyzed the same extract for lower-polarity organic chemistry using APPI in negative (−) and positive (+) ion modes (Fig. 1, B to D, and fig. S5), which show the same ranking in abundances of the chemical families but with lower importance of sulfur-bearing molecules. APPI enabled the ionization of oxygen-depleted and more unsaturated molecules (Fig. 1, B and C), with essentially one nitrogen or one sulfur heteroatom compared to ESI enabling the analysis of compounds rich in oxygen, nitrogen, and sulfur (fig. S4). APPI run in negative ionization mode [APPI(−)] particularly revealed 75% of CHO-type compounds and a subpopulation of aromatic highly oxygenized small molecules (all with a H/C ratio around 1). The regular pattern abundance observed in the van Krevelen diagram (Fig. 1B) suggests these being a homologous series of alkyl bi(tri)-phenyls substituted with increasing numbers of oxygen. APPI in positive ionization mode [APPI(+)] revealed the least oxygenated molecules involving 400 formulas of homologous series of hydrocarbons (CH) within a wide mass range [up to 850 u, atomic mass unit (amu)] and a wide range in saturation such as polycondensed aromatics (e.g., acenaphthene or fluorene) and many alkanes and olefins (with 9 to 60 carbons atoms) (Fig. 1D). The presence of polyaromatic hydrocarbons in Tissint had previously been shown by in situ techniques and attributed as martian (*15*).

In line with these MS results, the ^{1}H NMR spectrum of Tissint methanolic extract (fig. S5) demonstrated more details of a rich diversity of SOM, with 12.2% of terminal methyl (CCC$\mathbf{H}_3$, δ_H ~0.7 to 1.0 ppm), 6.6% of methyl within aliphatic units [—C—(C—C$\mathbf{H}_3$)—C—, δ_H ~1.0 to 1.2 ppm], 46.6% methylene and branched aliphatic units ($C_n\mathbf{H}_{2n+1}$, δ_H ~1.2 to 1.5 ppm), 8.5% (C$\beta\mathbf{H}_n$, δ_H ~1.5 to 1.9 ppm) and 9.8% (C$\alpha\mathbf{H}_n$, δ_H ~2.0 to 3.2 ppm) aliphatics proximate to carboxylic acids (HOOC—C$\alpha\mathbf{H}_n$—C$\beta\mathbf{H}_n$—), 12.7% OC$\mathbf{H}_n$ units (δ_H ~3.4 to 4.54 ppm), 2.0% of olefins (=C$\mathbf{H}_n$, δ_H ~5.0 to 6.0 ppm), and 1.7% of aromatic units ($C_{ar}\mathbf{H}$, δ_H ~6.0 to 8.4 ppm). Patterning of NMR resonances indicated projection of fundamental aliphatic patterns C_nH_{2n+1} (n ~3 to 7) of considerable diversity, with few proximate oxygen atoms. Considering the rather abundant OCH_n units [12.7% compared with 7.8% in Murchison methanolic extract (*29*)], the overall distribution of NMR resonances already suggested spatial separation of OCH_n from CCH_n units. The occurrence of extended aliphatic systems C_nH_{2n+1} in the presence of abundant OCH_n units implies some degree of convergence of OCH_n units, e.g., in the form of polyethers (—CHO—CHO— units). These have been observed in hydrothermally treated samples of Sutter's Mill meteorite (*35*), and hydrothermal alteration of organic molecules is perfectly conceivable under past and current martian mantle and crustal conditions as well as through impact ejection processes (*36*, *37*). The clustering of OCH_n groups among themselves and that a majority of those were not connected to aliphatic units were confirmed by a two-dimensional (2D) ^{1}H, ^{1}H total correlation spectroscopy (TOCSY) NMR spectrum (fig. S6).

DISCUSSION

Specific organic molecular diversity colocalized with mineral phases in Tissint meteorite

The Tissint meteorite is an Al-poor ferroan basaltic rock, rich in MgO and other compatible elements (Ni, Cr, and Co), similar to other depleted olivine-phyric shergottites, especially EETA 79001, with a total carbon/nitrogen abundance of 173/12.7 ppm of carbon/nitrogen [δ^{13}C: −26.6% (−12.8...−33.1%); δ^{15}N: −4.5% (−12.0...+17.3%)] (*23*, *26*). Tissint shows a rich internal mineral diversity that can be dissected in four major fractions (Fig. 2A):

1) Glazy black fusion crust formed during the transfer of the meteoroid through the terrestrial atmosphere;

2) Fine-grained interstitial main matrix composed of pyroxene-maskelynite (shocked plagioclase glass) with minor chromite $(Fe,Mg)Cr_2O_4$, ilmenite $FeTiO_3$, pyrrhotite $Fe_{1-x}S$, and phosphates;

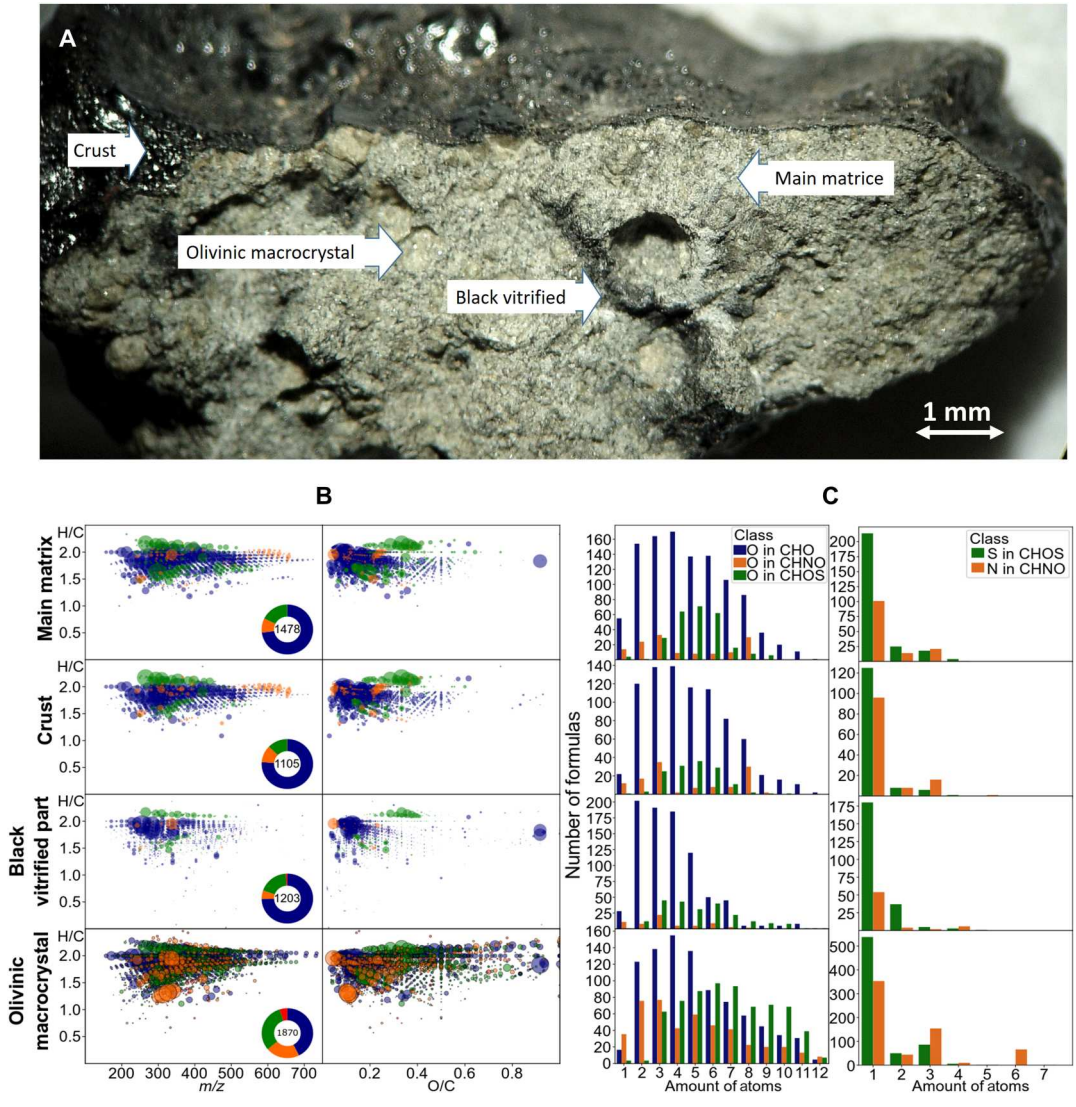

Fig. 2. Analysis details on a fractionated Tissint sample. (**A**) Differentiation of the four selected fraction in a small crusted Tissint fragment. (**B**) Molecular diversity in the methanol extracted fraction, derived from ESI(−) FTICR-MS spectra. Van Krevelen diagrams showing the relationships between *m/z*, O/C, and H/C corresponding to the annotated masses from the spectra. Dot color refers to CHO (blue), CHNO (orange), CHOS (green), and CHNOS (red); dot size refers to the intensity in the spectra. Pie plots in each diagram refer to portions of each chemical compound class and the total amount of compounds. (**C**) Bar charts of the four different parts of Tissint Mars meteorite showing the amounts of formulas (*y* axis) and corresponding amounts of oxygen, nitrogen, and sulfur (*x* axis) in the chemical compound classes of CHO, CHNO, and CHOS. Clearly visible is the higher abundance of oxygen-poor molecules in the olivine and the glassy part accompanied by compounds bearing up to four sulfur atoms.

3) Shock melt veins and pockets forming black vitrified material generated from shear melting during shock, colocalized with sulfur, probably as fine-grained sulfides (*26*);

4) Zoned olivinic macrocrystals up to 2 mm in length (*23*, *25*, *38*).

Spectral imaging of Tissint shown in this study (fig. S7) and that already in previous studies (*1*, *13*, *14*, *26*) had revealed several forms of abiotic carbonaceous matter with distinct Raman characteristics indicative of diverse composition and a high-temperature refractory component similar to that seen in Sheepbed mudstone. Most organic matter filled the fine veins (~10 μm, down to <1 μm) in olivines and pyroxene and the inclusions in pyroxenes and maskelynite, a common shock feature in Shergottites. Field-emission scanning electron microscopy (SEM) revealed submicron-sized grains and few aggregates with size up to 6 μm entrained in shock melt veins. Disaggregated pieces of the Tissint meteorite were placed under a microscope, and four different fractions were characterized, namely, (i) main matrix, (ii) crust, (iii) black vitrified material, and (iv) olivine macrocrysts. FTICR mass spectra of the methanolic extracts from all crushed fractions showed a remarkable disparity in the relative abundance and chemical diversity of its assigned molecular compositions of CHNOS and CHO(S)Mg compounds. In addition, polythionates ($[S_nO_6Na]^-$ ions with n = 3 to 9) and S6 sulfur ions were detected in ESI(−) spectra only in the main matrix and in much lesser amounts in the crust samples (fig. S8).

Each of the four fractions showed a very specific composition in the soluble organic signatures that may be directly connected to

their mineral rearrangements during formation, (shock) melt, and cooling. More than a thousand signals could be attributed to organomagnesium compositions from ESI(−) FTICR-MS analysis. The number of assigned molecular formula decreased in the order of olivine macrocrystals (1677) > main matrix (1478) > crust (1098) > the black vitrified material (717), with changing contributions of the various chemical homologous series in elemental compositions (CHO, CHNO, CHOS, CHNOS, CHOMg, and CHOSMg) (Fig. 2B). The olivine macrocrystals and the black vitrified material showed the highest counts of CHO and sulfur-containing molecules (CHOS), consistent with the observation of sulfur being confined in the shock melt veins, probably as fine-grained sulfides (*26*). Furthermore, these organic compounds showed less oxygenation than their precursors in the main matrix and a lower amount of polythiols in the veins, suggesting that both were possibly chemically reduced to the corresponding observed organo- and metal sulfides (Fig. 2C) during the shock melt. The crust and the main core matrix (constituting more than 80% of the original meteoritic material) are similar in their composition containing a predominance of CHO-bearing molecules (75%) and having substantial higher oxygenation than their corresponding CHO in the vitrified and olivine fractions. The organomagnesium compounds (CHOMg and CHOSMg) were shown to be stabilized carbon phases at high pressures and temperatures, respectively, in meteorites (*34*, *39*) and are most abundant in the shock-melted parts, the olivine macrocrystals and, to a lesser extent, in the crust (Fig. 3). The crust is derived mainly from the surface melting of the main matrix, and thus, these showed similar molecular profiles. The highest chemical abundance and diversity were observed in the olivine macrocrystals. In the olivine and in the strongly heated regions (shock melt veins and crust), an increase in organomagnesium is observed in strong correlation to a decrease in CHO compounds, attesting to their possible genetic linkage as illustrated in their close compositional profiles visualized in the compositional network in Fig. 3B and fig. S9.

APPI combined with ESI in FTICR-MS revealed a huge diversity in oxygen-poor carbon chemistry, such as alkylated polyaromatic hydrocarbons, alkanes, and olefins (Fig. 1D), which probably could be realized directly through abiotic synthesis mechanisms, such as Fisher-Tropsch–type or electrochemical reduction of CO_2. Their oxidation in various further steps including shock processing or continuing mineral interactions would facilitate the observed CHNOS molecular profile in oxygenation and thus in solubility of organic matter within the SOM versus insoluble organic matter continuum.

Various origins for pristine carbon–based molecules in Tissint and Mars meteorite include igneous synthesis, primary or secondary hydrothermal synthesis, and electrochemical synthesis, and exogenous sources (chondritic delivery) may have infiltrated into shock-induced fractures of the Tissint parent rock (*1*, *13*–*15*, *26*). Latest studies reported on organic synthesis associated with serpentinization and carbonation on early Mars (*12*) reveal the close relation of organic diversity and magnesium silicate coevolution. During cooling of the meteorite's parental melt, the olivine (magnesium silicates) is the first mineral to crystalize. Olivines and pyroxenes contain pockets (irregularities) and active crystal surfaces that, on interaction with a fluid, can conduct abiotic synthesis reactions. This can lead to the most complex heteroatom-rich and polyunsaturated molecules observed here, possibly also facilitated by the

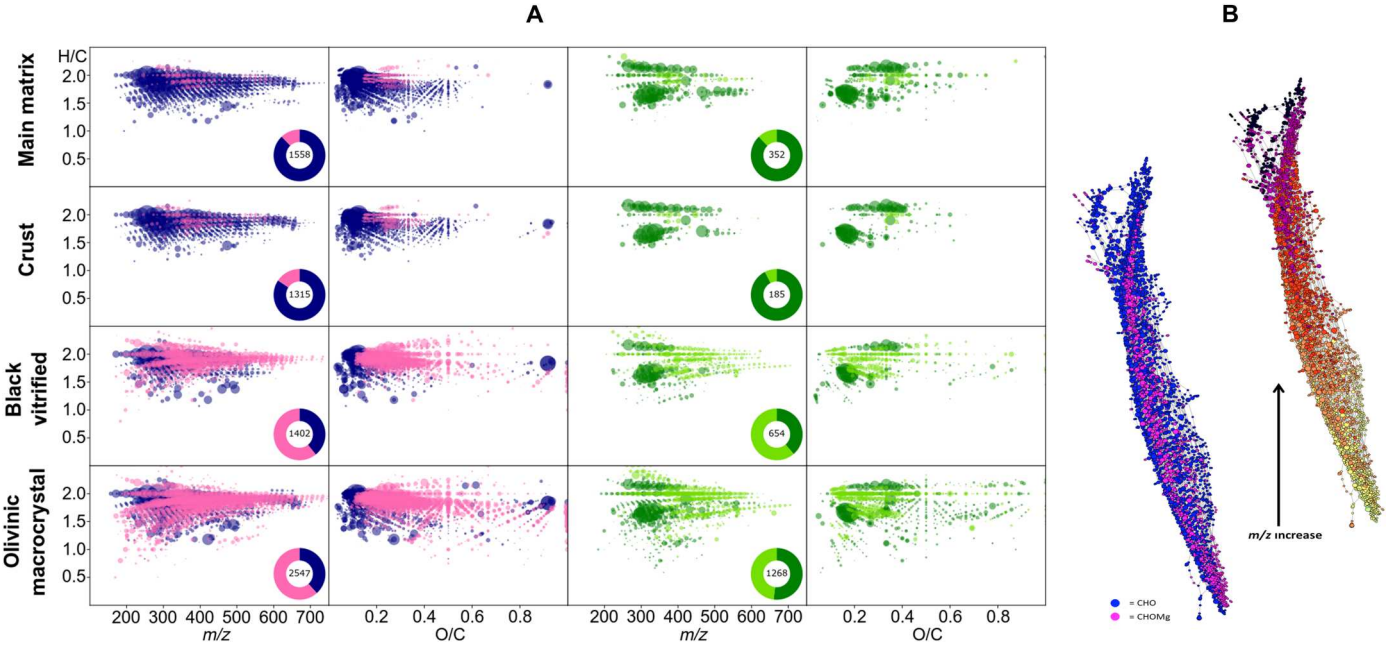

Fig. 3. Organomagnesium signatures in the different Tissint mineral fractions. (**A**) Molecular diversity in the methanol extracted fraction, derived from ESI(−) FTICR-MS spectra. Van Krevelen diagrams showing the relationships between *m/z*, O/C, and H/C corresponding to the annotated masses from the spectra. Dot color refers to CHO (blue), CHOMg (pink), CHOS (dark green), and CHOSMg (light green); dot size refers to the intensity in the spectra. Pie plots in each diagram refer to portions of each chemical compound class and the total amount of compounds. (**B**) Network of CHO and CHOMg compounds connected by mass differences. For this network, the mass differences of H_2, H_2O, H_2O_2Mg, CH_2, and O were used. The same network in different colors below shows the chemical evolution while *m/z* increases. Light colors (left) represent low masses (100 to 300 *m/z*), while dark colors (right) represent high masses (>500 *m/z*).

numerous heterocyclic coordination motifs available for unsaturated nitrogen and sulfur (CHN and CHS). The propensity of these heteroatoms to coordinate with metal species may also play a role. The fine-grained matrix, mainly composed of diaplectic feldspathic glass (maskelynite) and lower amount of pyroxenes, is poor in magnesium and, consequently, showed the least abundant and diverse suite of CHOMg compounds. We have observed selective enrichment of organomagnesium compounds in the olivine microcrystal phase; this may reflect an organic-rock (magnesium silicate) interaction after sequestration of the carbon phases into the meteorite's parental melt or selective formation of these molecules from the Mg-rich olivines during secondary aqueous processes prior high-temperature/shock events. Our results on diverse oxygenated carbon phases agree with earlier in situ analysis of melt inclusions in olivine from 13 martian meteorites, including Tissint and DAG476, in which reduced organic carbon was observed in the form of graphite and PAHs (*13*). Other early experiments on olivine described the presence of complex hydrocarbons and nitrogen-containing compounds in solvent extracts and similar molecules that were released upon heating to 550°C (*40*, *41*). Heterogeneous carbon distributions within single glass inclusion were also described in olivine from CV3 organic chondrites (*42*). The proportions of carbon in the oxidized group of olivine glasses (Bali, Allende, and Kaba) were threefold enriched relative to the reduced ones (e.g., Vigarano). The oxygenated carbon phases we observed in the Tissint olivine probably originate from multiparallel processes: (i) differential solubility of carbon in olivine dependent on pressure and temperature (as related to specific geological conditions at the ejecta site on Mars) and (ii) redox processes that affect the mineral and organic phases simultaneously in their conditions, adaptations, and evolution. Reduced carbon phases (e.g., graphite) with increasing carbon oxidation states from methane, alkanes, and olefinic hydrocarbons to polyaromatic hydrocarbon and graphite (as analyzed with APPI) are thermostable, can survive the melts, and could undergo further chemical redox reaction during cooling to reach the observed redox homeostasis. The oxidation of reduced carbon might occur in conjunction with the reduction of, for example, redox-active transition mineral ions and coordinating ligands under given kinetic and thermodynamic constraints. We found far fewer oxidized organic carbon occurrences in the olivine and the shock melts than in the main matrix of Tissint (Figs. 2B and 3A) along with a series of polythiols (S_3 to S_9) that occurred only in the main matrix and crust (fig. S8). This complex interplay between minerals and organic species may involve the reduction of iron and nickel in the presence of sulfur-containing compounds and sulfides to form iron/nickel sulfides. Demonstrating this idea, penthlandite [Fe(Ni,Fe)8S8] was indeed found closely associated with graphitic carbon in olivine inclusions of Allende (*43*) and associated with pyrite within Tissint (*15*). The presence of metal sulfide on Mars is well described along with their weathering at the oxidizing interphase with the atmosphere (*44*). Redox reactions with iron may also occur in interactions at interfaces with the olivine matrix itself, which is composed of Fe/Mg silicates (fayalite/forsterite). The prevalent association of organic material in inclusions of the Tissint meteorite is aromatic, aliphatic, and carbonyl/carboxyl organic material with magnetite and pyrrhotite in inclusions within maskelynite (*15*), and these incredible diversity and molecular speciation of the organic material were not previously reported.

We demonstrated the presence of a remarkably diverse suite of pristine reduced to oxidized carbon compounds in the Tissint Mars meteorite. Such a comprehensive description of organic diversity was never described previously from Mars meteorites or from any lander in situ on Mars. The organomagnesium CHO(S)Mg compounds were proximate to olivines, suggesting their formation close to the genesis of the magnesium silicate minerals. The origin of these complex organomagnesium compounds was previously related to high-temperature– and pressure-driven events in parent bodies and asteroids and may closely be aligned with the progression from the fluids/melts toward the microcrystals while cooling, reaching an organo-mineral redox homeostasis. The distinct footprint of soluble organic endogenous compounds in Tissint's lithology may also reflect site-specific geochemical processes on Mars and demonstrates an interconnection of the carbon cycle on Mars with sulfur cycles and mineral evolution. Furthermore, this knowledge of organomagnesium being present specifically in magnesium silicates corroborates ideally with the most recent results showing the colocalization of carbon with carbonate-bearing olivines (*45*) and, recently, the organic synthesis associated with serpentinization processes (*12*) involving the hydrolysis and transformation of primary ferromagnesian minerals, such as olivines and pyroxenes. This reflects the complex organic carbon signatures observed by the SAM instrument on Mars (*27*, *28*), bringing another hypothesis on the origin of organic matter on Mars.

Together, the differential CHONSMg-compositional footprints in the soluble organic phase of Tissint shed light into carbon sequestration mechanisms happening close to mineral history on a geological level already in deep mantle. Understanding in detail the correlation between the specific carbon and sulfur chemical diversity/complexity and its convergence with the mineral evolution/aqueous alteration becomes of major importance. This knowledge on carbon immobilization may also be important, especially for terrestrial systems where the abiotic carbon synthesis and sequestration in the deep zones are discussed with deep microbiomes to play an important role in a (global) carbon cycle and may explain a part of the yet-unknown carbon reservoirs.

MATERIALS AND METHODS

ESI-FTICR-MS experiments

Sample extraction and analysis followed standard operation procedures described earlier (*30*). Fragments of fresh interior samples (10 mg) were first washed by stirring for a few seconds within the extraction solvent (methanol, liquid chromatography–MS grade, Fluka) before crushing in 250 μl of solvent poured into the corresponding agate mortar. This procedure was shown to limit the number of peaks resulting from terrestrial and human contamination, for example, fatty acids arising from sample handling. The mixture (suspension) was transferred into an Eppendorf vial and underwent ultrasonic cleaning for <10 min and then was centrifuged. The supernatant liquid was removed with a microsyringe, ready for flow injection into the ESI source. A solvent methanolic blank was measured accordingly to be able to detect indigenous meteoritic (metal)organic matter in each sample.

The experimental study was performed on a high-field FTICR mass spectrometer from Bruker Daltonics with a 12-T magnet from Magnex. A time domain transient with 4 MWords was obtained and Fourier-transformed into a frequency domain spectrum.

The frequency domain was afterward converted to a mass spectrum by the SolariX Control program of Bruker Daltonics. The ion excitations were generated in broadband mode (frequency sweep radial ion excitation), and 3000 scans were accumulated for each mass spectrum in a mass range of m/z 147 to 1000. Ions were accumulated for 300 ms before ICR ion detection. The pressure in the quadrupole/hexapole and ICR vacuum chamber was 3×10^{-6} and 6×10^{-10} mbar, respectively. For collision-induced dissociation–tandem MS, ions were accumulated for 3 s.

The ESI source (Apollo II, Bruker Daltonics) was used in negative ionization mode. The methanolic solutions were injected directly into the ionization source by means of a microliter pump at a flow rate of 120 μl hour^{-1}. A source heating temperature of 200°C was maintained, and no nozzle-skimmer fragmentation was performed in the ionization source. The instrument was previously externally calibrated by using arginine-negative cluster ions (5 mg liter^{-1} of arginine in methanol).

FTICR mass spectra with m/z from 95 to 1000 amu were calibrated externally and internally to preclude alignment errors. Subsequently, the mass spectra were exported to peak lists at a signal-to-noise ratio ≥ 3. Elemental formulas were calculated combinatorically within a mass accuracy window of ±0.2 ppm for each peak in batch mode by an in-house software tool and validated via the senior-rule approach/cyclomatic number, assuming valence 2 for S and valence 4 (coordination number) for Mg.

FTICR-MS analysis enables highly resolved ($R > 10^6$ at m/z 200) and accurate chemical mass analysis of electrospray-generated ions within a 200–parts per billion error window over a wide mass range from m/z 100 to 1000. The weight of the ions is measured with a precision lower than the mass of an electron ($\Delta m/z = 0.0003$), and the specific signals can be differentiated with the same mass precision because of the ultrahigh resolution. These exact masses of the ions can routinely be converted into unique compositional formula bearing the light elements C—, H—, N—, O—, S—, and Mg (or any other element in target), also taking account of their natural isotopic abundance.

The SOM extracts generated thousands of individual signals that were converted into elementary compositions (formula); these are all represented in van Krevelen–type diagrams (H/C versus O/C) or related (H/C versus m/z), in which each formula is represented by a dot (the size of the dot is proportional to its abundance) as a projection of the relative oxygenation degree (O/C) and saturation degree (H/C) for various classes of compound types [CHO (blue), CHNO (orange), CHOS (dark green), CHNOS (red), CHOMg (pink), and CHOSMg (light green)]. Tissint was freshly collected after the fall and saved under clean conditions.

NMR analysis

The analysis followed that described previously with Murchison in (*30*). To resume, all experiments in this study were performed using a Bruker DMX 500 spectrometer at 283 K (CD_3OD) with a 5-mm z gradient $^1H/^{13}C/^{15}N$ TXI cryogenic probe using 90° excitation pulses (90° ð^{1}HÞ $^1/_4$ 10 μs, 90° ð^{13}CÞ $^1/_4$ 10 μs). 1D ^{1}H NMR was recorded using the first increment of the presaturation-nuclear Overhauser effect spectroscopy sequence (solvent suppression with presaturation and spinlock, 1-ms mixing time, 5-s acquisition time, 15-s relaxation delay, up to several hundred scans, and 1-Hz exponential line broadening). Absolute value correlation spectroscopy (COSY) and sensitivity-enhanced phase-sensitive TOCSY NMR spectra used spectral widths of 6009 Hz with acquisition times of 681 ms (relaxation delay, 819 ms for COSY and 2819 ms for TOCSY) and a dipsi2-mixing time of 70 ms; the number of scans was up to 512, and the number of increments was up to 1024. Sensitivity-enhanced ^{1}H, ^{13}C heteronuclear single-quantum coherence (HSQC) of methanolic extract used an acquisition time of 150 ms at a spectral width of 5482 Hz; ^{13}C-90° decoupling pulse, globally optimized alternating phase GARP (70 μs); 1JðCHÞ $^1/_4$ 150 Hz, 1.35-s relaxation delay; F1 (^{13}C), SW $^1/_4$ 22; 014 Hz (175 ppm); number of scans (F2)/F1 increments (^{13}C frequency) (512/406). Gradient (1-ms length and 450-μs recovery) and sensitivity-enhanced sequences were used for HSQC and TOCSY but not COSY spectra. References used were CD_3OD (3.30/49 ppm), CD_3CN (1.93 ppm), and CD_2Cl_2 (5.35 ppm). Homonuclear 2D NMR spectra were computed into an 8; 192 × 1; 024 matrix with exponential line broadening of 2.5 Hz in F2 and a shifted sine bell (π/2.5) in F1.

SEM-EDS Tissint

The matrix and an olivine macrocrystal of the Tissint meteorite were subjected to SEM and elemental analysis by EDX spectrometry (EDS). For the olivine sample, the mineral was broken to study the inner part. For both samples, the surface morphology of the uncoated sample was investigated using a Phenom ProX scanning electron microscope in backscattered electron mode. This instrument is equipped with an EDX spectrometer for analyzing the surface elements with a constant 15-kV accelerating voltage.

TG-DSC-MSEGA measurement conditions

Thermal measurements were performed on a Setaram LabsysEvo (Lyon, France) TG-DSC system, in flowing (90 ml/min) helium gas (99.9999% purity) atmosphere. The sample was weighed directly into a 100-μl Al_2O_3 crucible (the reference cell was empty) and was heated from 25° to 1000°C with a heating rate of 20°C/min. The obtained data were baseline-corrected and further processed with the thermoanalyzer′s processing software (Calisto Processing, version 2.092). The thermal analyzer (both the temperature scale and calorimetric sensitivity) was calibrated by a multipoint calibration method, in which seven different certified reference materials were used to cover the thermal analyzer′s entire operating temperature range. In parallel with the thermal measurements, the analysis of evolved gases/volatiles was performed on a Pfeiffer Vacuum Omni Star MSEGA system, which was connected to the abovementioned thermal analyzer. The gas splitter was thermostated to 220°C, while the transfer line to the mass spectrometer was thermostated to 200°C. The temperature of the mass spectrometer gas inlet was programmed to 120°C. The measurements were done in SEM bargraph cycles acquisition mode, where the m/z interval of 11 to 160 was continuously scanned with a speed of 20 ms/amu. The spectrometer was operated in electron impact mode.

Simultaneous TG-MSEGA analyses demonstrated the extremely low mass loss during the measurement. From room temperature up to 1000°C, only 0.06% of mass is lost in a narrow temperature range (340° to 460°C). Considering the MSEGA measurement results, it can be seen (fig. S3) from the start of the measurements that a slight decrease in the intensity of m/z – 44 signal is visible. The reason for this decrease is desorption and flushing of the carbon dioxide, which entered the furnace and gas transfer line during the sample loading into the TGA. Between 340° and 460°C, peaks are observable on m/z – 31, 39, 41, 44, and 56 discrete ion current curves, with

formation peak maxima at 400°C. The appearance of carbon dioxide in this temperature interval could be the result of catalytic oxidation, while the other four masses are the result of pyrolytic degradation of organics present in the meteorite matrix. The m/z − 31 could be CH_3O^+ or CH_2OH^+, which could form from methoxy derivatives, while the m/z − 39 ($C_3H_3^+$), 41 ($C_3H_5^+$), and 56 ($C_4H_8^+$) could form from the pyrolytic decomposition of some hydrocarbons. The slight mass increase (Δm + 0.0066%) between 500° and 680°C could be from the oxidation of the iron or, at such a low mass variation, could also be a small drift of the microbalance.

The mass decrease/loss continues above 700°C but at a much lower rate than at lower temperatures. This is mainly caused by the decomposition of some carbonates (see the peak on CO_2's molecular ion curve at 800°C) and sulfates or sulfites (observe the peaks on SO_2's molecular ion curve m/z64 at 770°C and the further rise of the curve above 860°C). The increasing tendency of the discrete ion chromatograms of the other masses (m/z − 15, 39, and 41) could be either due to some drift or they may really continue to form at higher temperatures, too.

Supplementary Materials

This PDF file includes:

Figs. S1 to S9

REFERENCES AND NOTES

1. J. L. Eigenbrode, R. E. Summons, A. Steele, C. Freissinet, M. Millan, R. Navarro-González, B. Sutter, A. C. McAdam, H. B. Franz, D. P. Glavin, P. D. Archer, P. R. Mahaffy, P. G. Conrad, J. A. Hurowitz, J. P. Grotzinger, S. Gupta, D. W. Ming, D. Y. Sumner, C. Szopa, C. Malespin, A. Buch, P. Coll, Organic matter preserved in 3-billion-year-old mudstones at Gale crater, Mars. *Science* **360**, 1096–1101 (2018).
2. H. Franz, P. Mahaffy, C. Webster, G. Flesch, E. Raaen, C. Freissinet, S. Atreya, C. House, A. McAdam, C. Knudson, P. D. Archer Jr., J. C. Stern, A. Steele, B. Sutter, J. L. Eigenbrode, D. P. Glavin, J. M. T. Lewis, C. A. Malespin, M. Millan, D. W. Ming, R. Navarro-González, R. E. Summons, Indigenous and exogenous organics and surface–atmosphere cycling inferred from carbon and oxygen isotopes at Gale crater. *Nat. Astron.* **4**, 526–532 (2020).
3. J. R. Michalski, T. C. Onstott, S. J. Mojzsis, J. Mustard, Q. H. Chan, P. B. Niles, S. S. Johnson, The martian subsurface as a potential window into the origin of life. *Nat. Geosci.* **11**, 21–26 (2018).
4. Y. L. Yung, P. Chen, K. Nealson, S. Atreya, P. Beckett, J. G. Blank, B. Ehlmann, J. Eiler, G. Etiope, J. G. Ferry, Methane on Mars and habitability: Challenges and responses. *Astrobiology* **18**, 1221–1242 (2018).
5. C. Szopa, C. Freissinet, D. P. Glavin, M. Millan, A. Buch, H. B. Franz, R. E. Summons, D. Y. Sumner, B. Sutter, J. L. Eigenbrode, First detections of dichlorobenzene isomers and trichloromethylpropane from organic matter indigenous to Mars mudstone in Gale crater, Mars: Results from the Sample Analysis at Mars instrument onboard the Curiosity rover. *Astrobiology* **20**, 292–306 (2020).
6. C. R. Webster, P. R. Mahaffy, S. K. Atreya, J. E. Moores, G. J. Flesch, C. Malespin, C. P. McKay, G. Martinez, C. L. Smith, J. Martin-Torres, J. Gomez-Elvira, M.-P. Zorzano, M. H. Wong, M. G. Trainer, A. Steele, D. Archer Jr., B. Sutter, P. J. Coll, C. Freissinet, P.-Y. Meslin, R. V. Gough, C. H. House, A. Pavlov, J. L. Eigenbrode, D. P. Glavin, J. C. Pearson, D. Keymeulen, L. E. Christensen, S. P. Schwenzer, R. Navarro-Gonzalez, J. Pla-García, S. C. R. Rafkin, Á. Vicente-Retortillo, H. Kahanpää, D. Viudez-Moreiras, M. D. Smith, A.-M. Harri, M. Genzer, D. M. Hassler, M. Lemmon, J. Crisp, S. P. Sander, R. W. Zurek, A. R. Vasavada, Background levels of methane in Mars' atmosphere show strong seasonal variations. *Science* **360**, 1093–1096 (2018).
7. I. P. Wright, M. M. Grady, C. T. Pillinger, Organic materials in a martian meteorite. *Nature* **340**, 220–222 (1989).
8. D. S. McKay, E. K. Gibson, K. L. Thomas-Keprta, H. Vali, C. S. Romanek, S. J. Clemett, X. D. Chillier, C. R. Maechling, R. N. Zare, Search for past life on Mars: Possible relic biogenic activity in martian meteorite ALH84001. *Science* **273**, 924–930 (1996).
9. J. Barrat, P. Gillet, M. Lesourd, J. Blichert-Toft, G. Poupeau, The Tatahouine diogenite: Mineralogical and chemical effects of sixty-three years of terrestrial residence. *Meteorit. Planet. Sci.* **34**, 91–97 (1999).
10. M. A. Sephton, Organic compounds in carbonaceous meteorites. *Nat. Prod. Rep.* **19**, 292–311 (2002).
11. A. Steele, F. M. McCubbin, M. D. Fries, D. C. Golden, D. W. Ming, L. G. Benning, Graphite in the martian meteorite Allan Hills 84001. *Am. Mineral.* **97**, 1256–1259 (2012).
12. A. Steele, L. G. Benning, R. Wirth, A. Schreiber, T. Araki, F. McCubbin, M. Fries, L. Nittler, J. Wang, L. Hallis, Organic synthesis associated with serpentinization and carbonation on early Mars. *Science* **375**, 172–177 (2022).
13. A. Steele, F. M. McCubbin, M. Fries, L. Kater, N. Z. Boctor, M. L. Fogel, P. G. Conrad, M. Glamoclija, M. Spencer, A. L. Morrow, M. R. Hammond, R. N. Zare, E. P. Vicenzi, S. Siljeström, R. Bowden, C. D. K. Herd, B. O. Mysen, S. B. Shirey, H. E. F. Amundsen, A. H. Treiman, E. S. Bullock, A. J. T. Jull, A reduced organic carbon component in martian basalts. *Science* **337**, 212–215 (2012).
14. A. Steele, F. M. McCubbin, M. D. Fries, The provenance, formation, and implications of reduced carbon phases in martian meteorites. *Meteorit. Planet. Sci.* **51**, 2203–2225 (2016).
15. A. Steele, L. G. Benning, R. Wirth, S. Siljeström, M. D. Fries, E. Hauri, P. G. Conrad, K. Rogers, J. Eigenbrode, A. Schreiber, A. Needham, J. H. Wang, F. M. McCubbin, D. Kilcoyne, J. D. Rodriguez Blanco, Organic synthesis on Mars by electrochemical reduction of CO_2. *Sci. Adv.* **4**, eaat5118 (2018).
16. C. Freissinet, D. P. Glavin, P. R. Mahaffy, K. E. Miller, J. L. Eigenbrode, R. E. Summons, A. E. Brunner, A. Buch, C. Szopa, P. D. Archer Jr., H. B. Franz, S. K. Atreya, W. B. Brinckerhoff, M. Cabane, P. Coll, P. G. Conrad, D. J. Des Marais, J. P. Dworkin, A. G. Fairén, P. François, J. P. Grotzinger, S. Kashyap, I. L. ten Kate, L. A. Leshin, C. A. Malespin, M. G. Martin, F. J. Martin-Torres, A. C. McAdam, D. W. Ming, R. Navarro-González, A. A. Pavlov, B. D. Prats, S. W. Squyres, A. Steele, J. C. Stern, D. Y. Sumner, B. Sutter, M. P. Zorzano; the MSL Science Team, Organic molecules in the Sheepbed Mudstone, Gale crater, Mars. *J. Geophys. Res. Planets* **120**, 495–514 (2015).
17. N. McLoughlin, E. G. Grosch, P. E. Vullum, P. Guagliardo, M. Saunders, D. Wacey, Critically testing olivine-hosted putative martian biosignatures in the Yamato 000593 meteorite—Geobiological implications. *Geobiology* **17**, 691–707 (2019).
18. C. B. Agee, N. V. Wilson, F. M. McCubbin, K. Ziegler, V. J. Polyak, Z. D. Sharp, Y. Asmerom, M. H. Nunn, R. Shaheen, M. H. Thiemens, A. Steele, M. L. Fogel, R. Bowden, M. Glamoclija, Z. Zhang, S. M. Elardo, Unique meteorite from Early Amazonian Mars: Water-rich basaltic breccia northwest Africa 7034. *Science* **339**, 780–785 (2013).
19. N. Castle, C. D. Herd, Experimental investigation into the effects of oxidation during petrogenesis of the Tissint meteorite. *Meteorit. Planet. Sci.* **53**, 1341–1363 (2018).
20. P. K. Byrne, A comparison of inner solar system volcanism. *Nat. Astron.* **4**, 321–327 (2020).
21. T. J. Lapen, M. Righter, R. Andreasen, A. J. Irving, A. M. Satkoski, B. L. Beard, K. Nishiizumi, A. T. Jull, M. W. Caffee, Two billion years of magmatism recorded from a single Mars meteorite ejection site. *Sci. Adv.* **3**, e1600922 (2017).
22. T. Schulz, P. P. Povinec, L. Ferrière, A. T. Jull, A. Kováčik, I. Sýkora, J. Tusch, C. Münker, D. Topa, C. Koeberl, The history of the Tissint meteorite, from its crystallization on Mars to its exposure in space: New geochemical, isotopic, and cosmogenic nuclide data. *Meteorit. Planet. Sci.* **55**, 294–311 (2020).
23. H. C. Aoudjehane, G. Avice, J. A. Barrat, O. Boudouma, G. Chen, M. J. M. Duke, I. A. Franchi, J. Gattacceca, M. M. Grady, R. C. Greenwood, C. D. K. Herd, R. Hewins, A. Jambon, B. Marty, P. Rochette, C. L. Smith, V. Sautter, A. Verchovsky, P. Weber, B. Zanda, Tissint martian meteorite: A fresh look at the interior, surface, and atmosphere of Mars. *Science* **338**, 785–788 (2012).
24. E. A. Jaramillo, S. H. Royle, M. W. Claire, S. P. Kounaves, M. A. Sephton, Indigenous organic-oxidized fluid interactions in the Tissint Mars meteorite. *Geophys. Res. Lett.* **46**, 3090–3098 (2019).
25. I. P. Baziotis, Y. Liu, P. S. DeCarli, H. J. Melosh, H. Y. McSween, R. J. Bodnar, L. A. Taylor, The Tissint martian meteorite as evidence for the largest impact excavation. *Nat. Commun.* **4**, 1–7 (2013).
26. Y. Lin, A. El Goresy, S. Hu, J. Zhang, P. Gillet, Y. Xu, J. Hao, M. Miyahara, Z. Ouyang, E. Ohtani, L. Xu, W. Yang, L. Feng, X. Zhao, J. Yang, S. Ozawa, NanoSIMS analysis of organic carbon from the Tissint martian meteorite: Evidence for the past existence of subsurface organic-bearing fluids on Mars. *Meteorit. Planet. Sci.* **49**, 2201–2218 (2014).
27. C. H. House, G. M. Wong, C. R. Webster, G. J. Flesch, H. B. Franz, J. C. Stern, A. Pavlov, S. K. Atreya, J. L. Eigenbrode, A. Gilbert, Depleted carbon isotope compositions observed at Gale crater, Mars. *Proc. Natl. Acad. Sci. U.S.A.* **119**, e2115651119 (2022).
28. B. Sutter, A. C. Mcadam, P. R. Mahaffy, D. W. Ming, K. S. Edgett, E. B. Rampe, J. L. Eigenbrode, H. B. Franz, C. Freissinet, J. P. Grotzinger, Evolved gas analyses of sedimentary rocks and eolian sediment in Gale crater, Mars: Results of the Curiosity rover's sample analysis at Mars instrument from Yellowknife Bay to the Namib Dune. *J. Geophys. Res. Planets* **122**, 2574–2609 (2017).

29. N. Hertkorn, M. Harir, P. Schmitt-Kopplin, Nontarget analysis of Murchison soluble organic matter by high-field NMR spectroscopy and FTICR mass spectrometry. *Magn. Reson. Chem.* **53**, 754–768 (2015).
30. P. Schmitt-Kopplin, Z. Gabelica, R. D. Gougeon, A. Fekete, B. Kanawati, M. Harir, I. Gebefuegi, G. Eckel, N. Hertkorn, High molecular diversity of extraterrestrial organic matter in Murchison meteorite revealed 40 years after its fall. *Proc. Natl. Acad. Sci. U.S.A.* **107**, 2763–2768 (2010).
31. A. Ruf, B. Kanawati, N. Hertkorn, Q. Z. Yin, F. Moritz, M. Harir, M. Lucio, B. Michalke, J. Wimpenny, S. Shilobreeva, B. Bronsky, V. Saraykin, Z. Gabelica, R. D. Gougeon, E. Quirico, S. Ralew, T. Jakubowski, H. Haack, M. Gonsior, P. Jenniskens, N. W. Hinman, P. Schmitt-Kopplin, Previously unknown class of metalorganic compounds revealed in meteorites. *Proc. Natl. Acad. Sci. U.S.A.* **114**, 2819–2824 (2017).
32. P. Jenniskens, A. E. Rubin, Q. Z. Yin, D. W. G. Sears, S. A. Sandford, M. E. Zolensky, A. N. Krot, L. Blair, D. Kane, J. Utas, R. Verish, J. M. Friedrich, J. Wimpenny, G. R. Eppich, K. Ziegler, K. L. Verosub, D. J. Rowland, J. Albers, P. S. Gural, B. Grigsby, M. D. Fries, R. Matson, M. Johnston, E. Silber, P. Brown, A. Yamakawa, M. E. Sanborn, M. Laubenstein, K. C. Welten, K. Nishiizumi, M. M. M. Meier, H. Busemann, P. Clay, M. W. Caffee, P. Schmitt-Kopplin, N. Hertkorn, D. P. Glavin, M. P. Callahan, J. P. Dworkin, Q. H. Wu, R. N. Zare, M. Grady, S. Verchovsky, V. Emel'yanenko, S. Naroenkov, D. L. Clark, B. Girten, P. S. Worden; The Novato Meteorite Consortium, Fall, recovery, and characterization of the Novato L6 chondrite breccia. *Meteorit. Planet. Sci.* **49**, 1388–1425 (2014).
33. O. P. Popova, P. Jenniskens, V. Emel'yanenko, A. Kartashova, E. Biryukov, S. Khaibrakhmanov, V. Shuvalov, Y. Rybnov, A. Dudorov, V. I. Grokhovsky, D. D. Badyukov, Q.-Z. Yin, P. S. Gural, J. Albers, M. Granvik, L. G. Evers, J. Kuiper, V. Kharlamov, A. Solovyov, Y. S. Rusakov, S. Korotkiy, I. Serdyuk, A. V. Korochantsev, M. Y. Larionov, D. Glazachev, A. E. Mayer, G. Gisler, S. V. Gladkovsky, J. Wimpenny, M. E. Sanborn, A. Yamakawa, K. L. Verosub, D. J. Rowland, S. Roeske, N. W. Botto, J. M. Friedrich, M. E. Zolensky, L. Le, D. Ross, K. Ziegler, T. Nakamura, I. Ahn, J. I. Lee, Q. Zhou, X.-H. Li, Q.-L. Li, Y. Liu, G.-Q. Tang, T. Hiroi, D. Sears, I. A. Weinstein, A. S. Vokhmintsev, A. V. Ishchenko, P. Schmitt-Kopplin, N. Hertkorn, K. Nagao, M. K. Haba, M. Komatsu, T. Mikouchi; Chelyabinsk Airburst Consortium, Chelyabinsk airburst, damage assessment, meteorite recovery, and characterization. *Science* **342**, 1069–1073 (2013).
34. M. Matzka, M. Lucio, B. Kanawati, E. Quirico, L. Bonal, S. Loehle, P. Schmitt-Kopplin, Thermal history of asteroid parent bodies is reflected in their metalorganic chemistry. *Astrophys. J. Lett.* **915**, L7 (2021).
35. S. Pizzarello, S. K. Davidowski, G. P. Holland, L. B. Williams, Processing of meteoritic organic materials as a possible analog of early molecular evolution in planetary environments. *Proc. Natl. Acad. Sci. U.S.A.* **110**, 15614–15619 (2013).
36. H. Lammer, E. Chassefière, Ö. Karatekin, A. Morschhauser, P. B. Niles, O. Mousis, P. Odert, V. U. Möstl, D. Breuer, V. Dehant, M. Grott, H. Gröller, E. Hauber, L. B. S. Pham, Outgassing history and escape of the martian atmosphere and water inventory. *Space Sci. Rev.* **174**, 113–154 (2013).
37. L. M. Parro, A. Jiménez-Díaz, F. Mansilla, J. Ruiz Pérez, Present-day heat flow model of Mars. *Sci. Rep.* **7**, 1–9 (2017).
38. A. Basu Sarbadhikari, E. V. S. S. K. Babu, T. Vijaya Kumar, H. Chennaoui Aoudjehane, Martian meteorite Tissint records unique petrogenesis among the depleted shergottites. *Meteorit. Planet. Sci.* **51**, 1588–1610 (2016).
39. A. Ruf, L. L. d'Hendecourt, P. Schmitt-Kopplin, Data-driven astrochemistry: One step further within the origin of life puzzle. *eLife* **8**, 18 (2018).
40. F. Freund, A. Gupta, D. Kumar, in *Lunar and Planetary Science Conference* (1996), vol. 27.
41. R. Knobel, H. Breuer, F. Freund, Abiotic synthesis of organic molecules from minerals containing traces of dissolved H_2O, CO_2 and N_2 part II: Experimental data. *Orig. Life* **14**, 197–204 (1984).
42. M. E. Varela, N. Metrich, M. Bonnin-Mosbah, G. Kurat, Carbon in glass inclusions of Allende, Vigarano, Bali, and Kaba (CV3) olivines. *Geochim. Cosmochim. Acta* **64**, 3923–3930 (2000).
43. A. J. Brearley, Origin of graphitic carbon and pentlandite in matrix olivines in the allende meteorite. *Science* **285**, 1380–1382 (1999).
44. D. Fisher, J. Burns, K. Pond, Estimation of mean and median particle size of ruminant digesta. *J. Dairy Sci.* **71**, 518–524 (1988).
45. C. S. Edwards, B. L. Ehlmann, Carbon sequestration on Mars. *Geology* **43**, 863–866 (2015).

Acknowledgments

Funding: This work was funded by the Deutsche Forschungsgemeinschaft (DFG, German Research Foundation) Project-ID 364653263–TRR 235 (CRC 235). **Author contributions:** Conceptualization: P.S.-K. Methodology: P.S.-K., M.M., A.R., N.H., M.L., J.H., M.H., B.M., R.D.G., V.H., N.W.H., and A.S. Investigation: P.S.-K., M.M., A.R., A.S., L.F., A.G., Z.G., and H.C.A. Visualization: P.S.-K., M.M., A.R., N.H., J.H., and M.H. Samples: P.S.-K., A.S., A.G., L.F., H.C.A., and Z.G. Funding acquisition: P.S.-K. Project administration: P.S.-K. Supervision: P.S.-K. Writing—original draft: P.S.-K. Writing—review and editing: all authors. **Competing interests:** The authors declare that they have no competing interests. **Data and materials availability:** All data needed to evaluate the conclusions in the paper are present in the paper and/or the Supplementary Materials.

Submitted 24 June 2022
Accepted 12 December 2022
Published 11 January 2023
10.1126/sciadv.add6439